

MEMS-Based Hemispherical Resonator Gyroscopes

P. Pai, F. K. Chowdhury, Carlos H. Mastrangelo and M. Tabib-Azar

Electrical and Computer Engineering
University of Utah
Salt Lake City, USA
azar.m@utah.edu

Abstract— This paper introduces a fabrication technique that uses planar MEMS micromachining processes to produce hemispherical resonating shells for gyroscopes. The hemispheres exhibit a quality factor in excess of 20,000 with resonant frequencies in the range of 20 kHz for the 4-node wineglass mode. The fabrication process enables production of almost perfect hemispheres (less than 1% asphericity near the pedestal) with an average surface roughness of 5nm. The high degree of sphericity contains the relative frequency mismatch $\Delta f/f$ between the two degenerate modes to 0.02%. Simplicity of the fabrication process and the successful testing of the drive/sense mechanism in the resonator make it a good candidate for use as gyroscopes.

I. INTRODUCTION

MEMS process has been used in the past to fabricate a variety of gyroscopes. The basic working principle among these gyroscopes involves sensing the Coriolis force on a vibrating suspended mass. Different structural designs for the gyroscope reported in the past include cantilever [1], tuning fork [2], gimbal [3] and inter-digital electrodes [4]. The driving/sensing schemes for these designs are varied, among which electrostatic, electromagnetic, piezoelectric and piezoresistive are popular. Due to the fabrication imperfections associated with MEMS process, it is difficult to produce perfectly symmetric structures for complex structures like gimbal and inter-digital electrodes. This adversely affects the frequency matching and quality factor of the device, creating a need for post-fabrication trimming and tuning. It is therefore desirable to use structures that are inherently symmetric like a disc, hemisphere and sphere; instead of designing one.

Wineglass resonators have been popular as gyroscopes in aviation and space exploration due to their extremely high Q-factor and inherent structural symmetry. Hemispherical resonator gyroscopes (HRG) functioning in the wineglass resonance mode have exhibited Q-factor as high as 26 million at macro-scale [5]. HRGs can be stemmed or stem-less in design. This work focuses on the stem-less design and any mention of HRG henceforth will refer to the stem-less. Majority of the commercially available HRGs consist of relatively large individually manufactured wineglass structures that are assembled into a drive/sense package for operation. Recently, micro-scale glass-blowing has been used

to create 3-D spherical-shell resonators [6]. These shells produced Q-factor in the range of 500, which is large considering their operation in air. The successful demonstration of the working of these shells provides hope in directing efforts to produce 3-D MEMS structures. Wineglass resonator based on MEMS has been reported in the past, which is limited to simple 2-D ring structure [7].

This work introduces a simple MEMS process that produces 3-D hemispherical structures with integrated electrodes. The process resulted in nearly perfect hemispherical shell with rms surface roughness of 5nm. Testing of these shells showed Q-factor of the order of 20,000 in 50mT vacuum. The shells were tested with different driving/sensing schemes that are reported in this work.

II. DESIGN AND FABRICATION

The design consists of a silicon dioxide hemispherical shell 500 μ m in diameter that is anchored to the substrate. The electrodes for driving/sensing are symmetrically placed on the periphery of the shell, separated by a distance defined by the sacrificial layer thickness (figure 1). Figure 2 schematically explains the working principle of the device in the 4-node resonance mode. A pair of “driving electrodes” capacitively couple the actuation signal to the shell. A second pair of “sensing electrodes” placed orthogonal to the “driving electrodes” pickup the vibrations from the shell. The shell, substrate and the electrodes are all electrically isolated from one another.

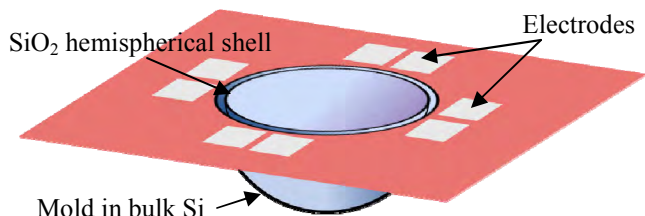


Figure 1: Schematic representation of the HRG design.

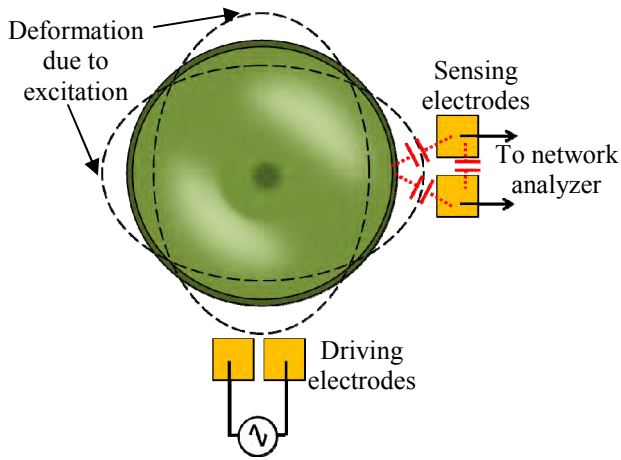


Figure 2: Top view schematic representation of the working principle of the HRG in the 4-node resonance mode. Figure not drawn to scale.

Fabrication of the HRGs (Fig. 3) began on a $4\text{ }\square$ silicon wafer passivated with a 500nm low stress LPCVD silicon nitride layer onto which circular openings were etched using RIE. The next stages involved isotropic etching of the Si substrate in a (1:9) mixture of 49% HF and 60% HNO_3 following procedures reported by [8]. The nitride mask was removed after the hemispherical mold was created. The wafer was then subject to thermal oxidation to serve as an etch stop against XeF_2 during the sacrificial etch. Thereafter, Al electrodes were patterned around the perimeter of the etched mold followed by sputter deposition of sacrificial amorphous silicon of thickness $1\text{ }\mu\text{m}$. Next, openings for pedestals/anchors (to support the final structure) were etched into the center of the mold. Finally, the actual layer that formed the hemispherical resonator was deposited by sputtering $1\text{ }\mu\text{m}$ SiO_2 and patterning/etching them around the circumference of the mold. This was followed by XeF_2 etch of the sacrificial layer resulting in free-standing SiO_2 hemispherical shells supported on pedestals. Figure 4 shows an optical image of the top-view of a HRG.

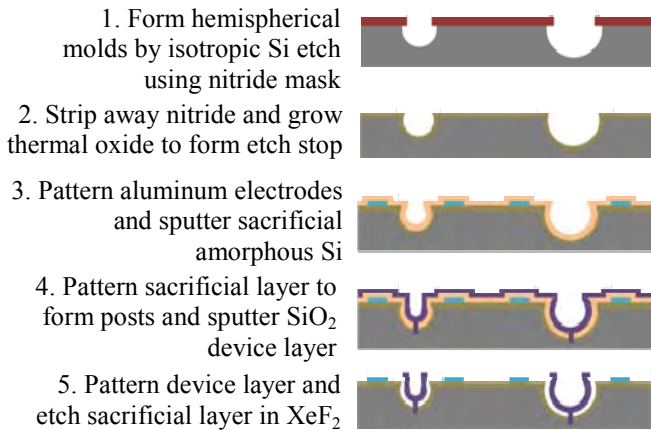


Figure 3: Sideview of the fabrication process flow for the HRG.

III. MEASUREMENT TECHNIQUES

The hemispherical resonator was tested using three different schemes viz. electrostatic driving/sensing (a), piezoelectric enhanced electrostatic driving/electrostatic sensing (b) and electrostatic driving/optical sensing (c).

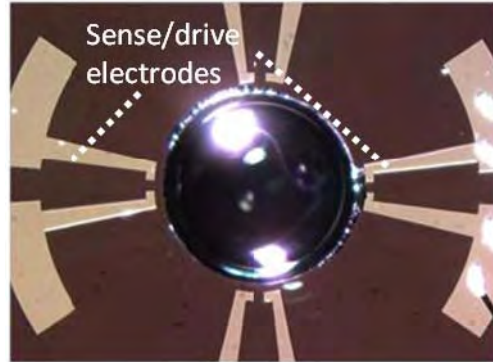


Figure 4: Optical image of the top-view of a HRG with integrated electrodes.

A. Electrostatic driving/sensing

This technique used only one pair of electrodes to drive/sense the vibrations at resonance (figure 5). The method was based on the assumption that the amplified white noise from differential amplifier was sufficient to create a small mechanical disturbance on the HRG shell. The HRG would then respond to only its natural frequency and couple signal back to the second electrode in the pair, which was connected to the input of the differential amplifier. The HRG attained a stable state of oscillations as the noise made several passes through the filtered positive-feedback loop. The output of the amplifier was read out in an Agilent 4395 A network/spectrum analyzer.

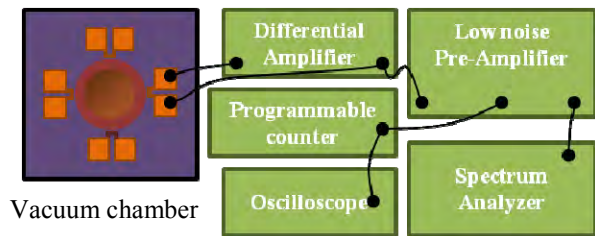


Figure 5: Schematic representation of the measurement technique (a) that used electrostatic force for driving/sensing. Driving/sensing is achieved with two electrodes from the same pair. A positive-feedback loop is formed with the HRG acting as a filter.

B. Piezoelectric enhanced electrostatic driving/electrostatic sensing

Figure 6 shows a schematic representation of this technique. This technique was an attempt to increase the Q-factor of the HRG. The HRG die was fixed on a plexi-glass cube with piezoelectric discs attached to its face. Two orthogonally placed pairs of electrodes were placed in a positive-feedback loop like in (a) and the output was read out in a network analyzer. Only one of the piezoelectric discs aligned to the driving electrodes was actuated during operation.

C. Electrostatic driving/optical sensing

The setup used an external probe tip to excite the shell through a signal generator. The probe was used to enhance the capacitive coupling through increased overlap area. A laser source was used to illuminate the rim of the shell. The light reflected from the shell was collected and converted to electric signal in a photomultiplier tube. Optic fibers were used to both shine and receive light. Figure 7 shows a graphic representation of the setup.

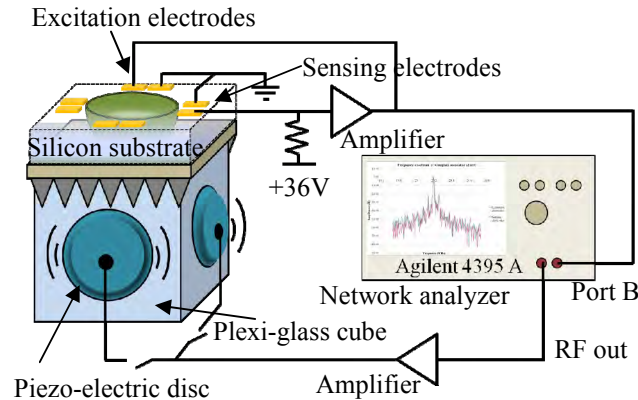


Figure 6: Schematic representation of the measurement technique (b) that used piezoelectric driving/electrostatic sensing. Only one of the piezoelectric discs was actuated during measurement. Two pairs of orthogonally placed electrodes were placed in a positive-feedback loop for driving/sensing.

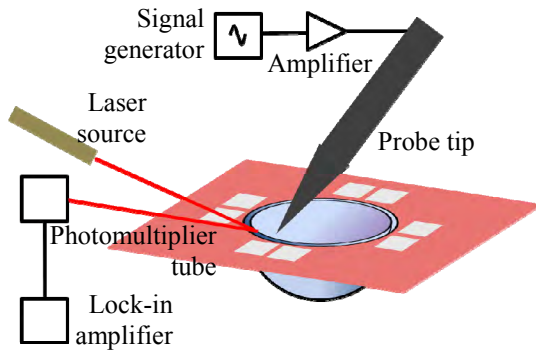


Figure 7: Schematic representation of the measurement setup for technique (c). The probe tip was used to electrostatically actuate the hemispherical shell. The vibrations were picked up using the optical setup.

IV. RESULTS

The hemispherical shells were scanned in a Cypher AFM for surface roughness and showed less than 5nm of rms surface roughness across a $20\mu\text{m} \times 20\mu\text{m}$ area. Figure 8 shows SEM images, curve tracing and surface roughness scans of the hemispherical shell. The cross-section scan of the shell showed less than 1% deviation from a perfect semi-circle near the pedestal region. The result is also corroborated by earlier reports that used the same technique in creating molds for microlens [8].

Technique (a) produced a resonant peak at 21.9kHz (figure 9(a)) that closely matches the resonant frequency of 22KHz, obtained through numerical simulation. The quality factor obtained through this technique was 22k. The mismatch in the resonant frequencies of two degenerate modes is clearly

visible in figure 9(a) in the form of split peaks separated by 5Hz.

Technique (b) produced a resonant peak at 24kHz, which deviates from the simulation results (figure 10). This indicates that the peak obtained is for a mode different from the 4-node wineglass mode. The piezoelectric actuation could have created significant vibrations to dampen the 4-node mode and slightly enhance a different mode.

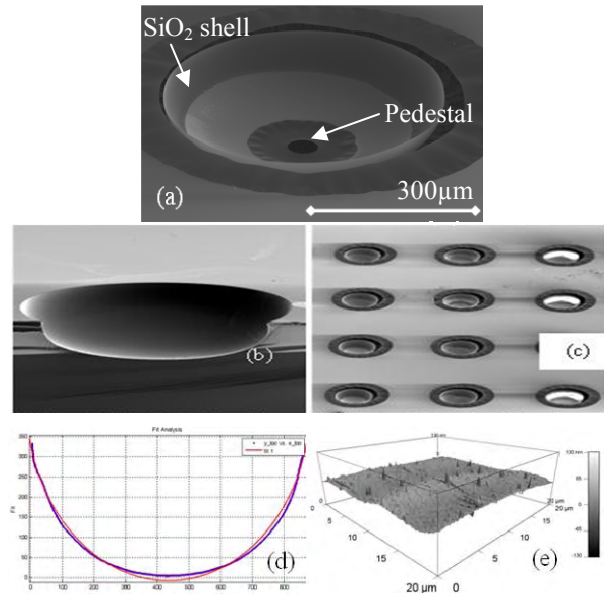


Figure 8: SEM Images of hemispherical resonator shells a) close up of final device with shell and pedestal, b) SEM of mold formed via isotropic silicon etch, c) wafer-scale batch fabrication of HRG SiO_2 shell, d) cross-section of hemisphere fit with a semi-circle with deviation less than 1% near the stem and e) AFM scan of shell surface showing less than 5 nm rms roughness.

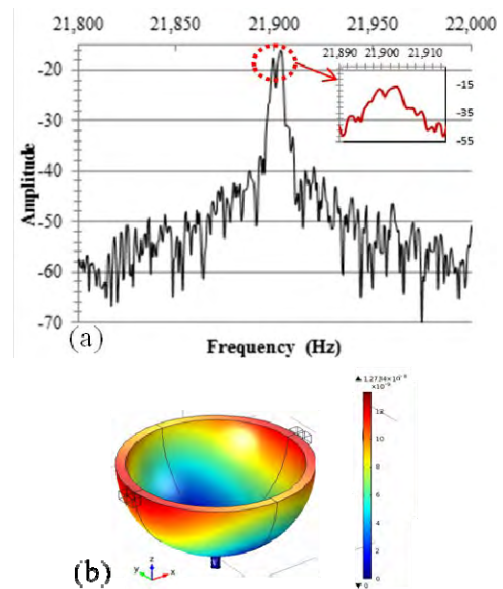


Figure 9: (a) Frequency plot from spectrum analyzer for technique (a). (b) Snapshot of the COMSOL animation showing displacement of the shell during resonance.

Technique (c) resulted in multiple peaks owing to different modes of vibration (figure 11). The multiple peaks arise due to the enhanced cross-coupling due to wider area coverage by the external probe tip compared against the integrated electrodes in the techniques (a), (b). Also, it can be seen that the 4-node wineglass resonant frequency (~22kHz) is suppressed compared against the resonant frequencies of other modes.

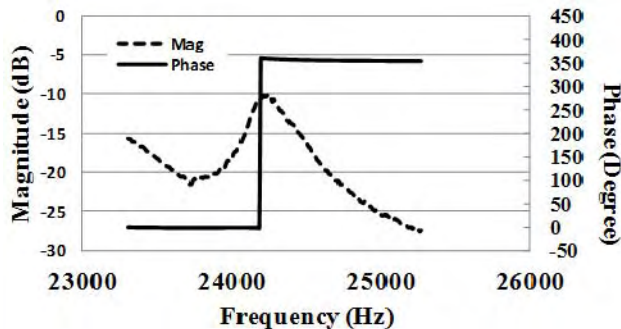


Figure 10: Frequency characterization plot for the measurement technique (b).

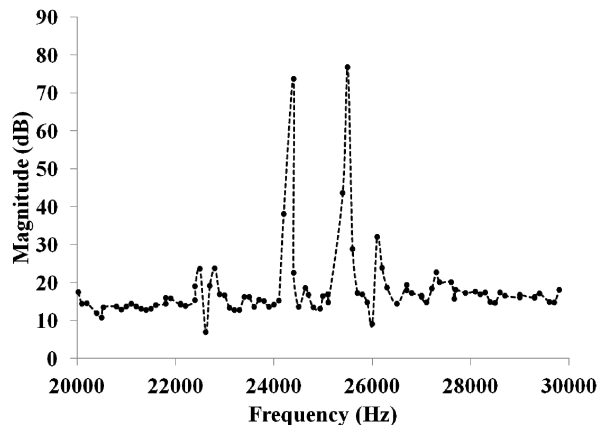


Figure 11: Network analyzer frequency sweep for technique (c). Multiple peaks observed due to enhanced cross-coupling owing to larger overlap area from the external probe electrode.

V. CONCLUSION

We successfully demonstrate for the first time, fabrication of 3-D hemispherical resonators using planar MEMS process.

The hemispherical shells produced have less than 1% asphericity in the pedestal region and the average surface roughness is within 5nm. Three different techniques were tried in testing the resonators and the best results obtained were from the electrostatic driving/sensing scheme. Q-factor of 22000 was achieved under a vacuum level of 50mT with this technique. Other ALD and ultra-low thermal expansion layers for the shells are currently being developed. Efforts are also being directed at suppressing the vibrations from undesired modes and improving Q-factor.

ACKNOWLEDGMENT

This work was supported by DARPA μ HRG Program grant W31P4Q-11-1-0010 under Dr. Andrei Shkel. Mr. Y. Chen contributed to the simulation results in Fig. 9b.

REFERENCES

- [1] K. Maenaka, T. Fujita, Y. Konishi and M. Maeda, "Analysis of a Highly Sensitive Silicon Gyroscope with Cantilever Beam as Vibrating Mass", *Sensors and Actuators A*, Vol. 54, p. 568-573, 1996.
- [2] R. Voss et al, "Silicon Angular Rate Sensor for Automotive Applications with Piezoelectric Drive and Piezoresistive Read-out", *Transducers*, p. 879-882, 1997.
- [3] K. Maenaka, S. Ioku, N. Sawai, T. Fujita and Y. Takayama, "Design, Fabrication and Operation of MEMS Gimbal Gyroscope", *Sensors and Actuators A*, Vol. 121, p. 6-15, 2005.
- [4] H. Oh, W. Wang, S. Yang and K. Lee, "Development of SAW Based Gyroscope with High Shock and Thermal Stability", *Sensors and Actuators A*, Vol. 165, p. 8-15, 2011.
- [5] D. M. Rozelle, "The Hemispherical Resonator Gyro: From Wineglass to the Planets", *Proc. 19th AAS/AIAA Space Flight Mechanics Meeting*, p. 1157-1178, 2009.
- [6] I. P. Prikhodko, S. A. Zotov, A. A. Trusov and A. M. Shkel, "Microscale Glass-blown Three-dimensional Spherical Shell Resonators", *Journal of Microelectromechanical Systems*, Vol. 20, p. 691-701, 2011.
- [7] Y. Xie, S. Li, Y. Lin, Z. Ren and C. T. Nguyen, "1.52-GHz Micromechanical Extensional Wine-glass Mode Ring Resonators", *IEEE Transactions on Ultrasonics, Ferroelectrics and Frequency Control*, Vol. 55, p. 890-907, 2008.
- [8] J. Albero, *et al.*, "Fabrication of spherical microlenses by a combination of isotropic wet etching of silicon and molding techniques," *Opt. Express*, vol. 17, p. 6283-6292, 2009.